

# Optimize Nonlinear Beam Dynamical System with Square Matrix Method

Yongjun Li,\* Li Hua Yu, and Lingyun Yang†  
*Brookhaven National Laboratory, Upton, New York 11973*

Nonlinear dynamics has an important role when designing modern synchrotron lattices. In this letter, we introduce a new method of using a square matrix to analyze periodic nonlinear dynamical systems [1, 2]. Applying the method to the National Synchrotron Light Source II storage ring lattice has helped to mitigate the chaotic motion within its dynamic aperture. For a given dynamical system, the vector space of a square matrix can be separated into different low dimension invariant subspaces according to their eigenvalues. When Jordan decomposition is applied to one of the eigenspaces, it yields a set of accurate action-angle variables. The distortion of the new action-angle variables provides a measure of the nonlinearity. Our studies show that the common convention of confining the tune-shift with amplitude to avoid the crossing of resonance lines may not be absolutely necessary. We demonstrate that the third order resonance can be almost perfectly compensated with this technique. The method itself is general, and could be applied to other nonlinear systems.

## I. INTRODUCTION

Long-term nonlinear behavior of charged particles in synchrotron plays a vital role in beam dynamics. To understand the impact nonlinear behavior has, one can analyze particle motion under many iterations of the one-turn-map. The reliable numerical approach is using appropriate local symplectic integration methods [3–5]. For the analysis of the dynamics, however, one can use a more compact representation of the one-turn-map to extract relevant information. There are many approaches one can take, such as canonical perturbation theory, Lie operators, power series, and normal form[6–21], etc. Here, we would like to study this problem from a somewhat different perspective (i.e., using linear algebra techniques.) The detailed theory on the method has been explained in ref. [1, 2]. We will summarize this method in Section II, and then describe its applications in Section III.

## II. THEORY

For a given periodic system, such as a particle moving in a synchrotron, its status can be represented by the complex normalized variable [10, 12, 22, 23]  $z = \bar{x} - i\bar{p} = \sqrt{2J}e^{i\psi}$  and its conjugate  $z^* = \bar{x} + i\bar{p} = \sqrt{2J}e^{-i\psi}$ . We use these to form a truncated vector  $\mathbf{Z} = (1, z, z^*, z^2, zz^*, \dots, z^{*n})^T$ , where  $(J, \psi)$  are linear action-angle variables,  $T$  is the vector transpose, and  $n$  is the truncated order. The one-turn-map from an initial status  $\mathbf{Z}_0$  to its final status  $\mathbf{Z}_1$  is represented by a square matrix  $\mathbf{M}$ :

$$\mathbf{Z}_1 = \mathbf{M}\mathbf{Z}_0. \quad (1)$$

The matrix  $\mathbf{M}$  is upper-triangular, and has the form

$$\mathbf{M} = \begin{pmatrix} 1 & 0 & \cdots & 0 \\ 0 & \mathbf{M}_{11} & \cdots & \mathbf{M}_{1n} \\ \vdots & 0 & \ddots & \vdots \\ 0 & 0 & \cdots & \mathbf{M}_{nn} \end{pmatrix}. \quad (2)$$

Here different submatrices  $\mathbf{M}_{ij}$  have different dimensions. All diagonal blocks  $\mathbf{M}_{ii}$ 's are square diagonal submatrices.

Since the matrix is upper-triangular, its eigenvalues are given by its diagonal elements in the form of  $e^{im\mu}$ , where  $m$  is an integer, and  $\mu$  is the linear tune. We can separate the full space spanned by the matrix columns into different invariant subspaces according to the eigenvalues. We found that the simplest invariant subspace  $e^{i\mu}$  already provides a wealth of information about the dynamical system and the high dimension matrix is reduced to a much lower dimension. For example, for a 7<sup>th</sup> order 4D phase space system, its original dimension is  $330 \times 330$ . After Jordan decomposition, a set of 4 left-eigenvectors  $\mathbf{u}_{k=0,\dots,3}$  span the invariant subspace  $e^{i\mu}$ . A matrix  $\mathbf{U}$  consists of these 4 row vectors satisfies the left-eigenvector equation

$$\mathbf{U}\mathbf{M} = e^{i\mu}\mathbf{I} + \tau \mathbf{U} = \mathbf{N}\mathbf{U} \quad (3)$$

where the  $4 \times 4$  matrix  $\mathbf{N}$  is the Jordan block with the eigenvalue  $e^{i\mu}$ , corresponding to the  $e^{i\mu}$  invariant subspace inside the space of vector  $\mathbf{Z}$ .  $\mathbf{I}$  is the identity matrix in this space, while  $\tau$  is a superdiagonal matrix:

$$\tau = \begin{pmatrix} 0 & 1 & & \\ & 0 & \ddots & \\ & & \ddots & 1 \\ & & & 0 \end{pmatrix}. \quad (4)$$

The mapping from  $\mathbf{Z}_0$  to  $\mathbf{Z}_1$  generated by the one-turn-map  $\mathbf{M}$ , when projected into this subspace, can be re-written as

$$\mathbf{W}_1 \equiv \mathbf{U}\mathbf{Z}_1 = \mathbf{U}\mathbf{M}\mathbf{Z}_0 = e^{i\mu}\mathbf{I} + \tau \mathbf{U}\mathbf{Z}_0 \equiv e^{i\mu}\mathbf{I} + \tau \mathbf{W}_0. \quad (5)$$

\* yli@bnl.gov

† Currently at Renaissance Technologies LLC.

$\mathbf{W}_0$  can be written as a one-column vector

$$\mathbf{W}_0^T = (w_0, w_1, w_2, \dots, w_{m-1}), \quad (6)$$

where  $m$  is the dimension of the invariant subspace. KAM theory states that the invariant tori are stable under small perturbation [6, 13, 24]. For sufficiently small amplitude of oscillation in  $\mathbf{Z}$ , the invariant tori are deformed and survive. So the system has a nearly stable frequency and when the amplitude is small, the fluctuation of the frequency is also small. Thus for a specific initial condition described by  $\mathbf{Z}_0$ , the rotation in the eigenspace should be represented by a phase factor  $e^{i(\mu+\phi)}$  as

$$\mathbf{W}_1 = e^{i\mu\mathbf{I}+\tau}\mathbf{W}_0 \cong e^{i(\mu+\phi)}\mathbf{W}_0. \quad (7)$$

where  $\phi$  depends on the initial condition.

$\tau$  in Eq. (4) has no proper eigenvector, but only generalized eigenvectors. However, as we increase the order of the Taylor expansion, the dimension of the eigenspace increases and approaches infinity, and the eigenvector of  $\tau$  is defined as a coherent state [25, 26]:

$$\tau\mathbf{W}_0 \cong i\phi\mathbf{W}_0. \quad (8)$$

The polynomials in Eq. (6) are  $w_0 = u_0\mathbf{Z}_0, w_1 = u_1\mathbf{Z}_0, w_2 = u_2\mathbf{Z}_0, \dots$ . Then Eq. (8) reads as

$$\tau \begin{pmatrix} w_0 \\ w_1 \\ \vdots \\ w_{m-1} \end{pmatrix} = \begin{pmatrix} w_1 \\ w_2 \\ \vdots \\ 0 \end{pmatrix} \cong \begin{pmatrix} i\phi w_0 \\ i\phi w_1 \\ \vdots \\ i\phi w_{m-1} \end{pmatrix}. \quad (9)$$

When the invariant tori survive and there is a stable frequency, we see that Eq. (9) requires

$$i\phi = \frac{w_1}{w_0} \cong \frac{w_2}{w_1} \dots \cong \frac{w_{m-1}}{w_{m-2}}. \quad (10)$$

Therefore only those vectors  $\mathbf{W}_0$  which satisfy Eq. (10) with  $\phi$  as a real number represent a motion with a stable frequency given by a phase advance  $\mu + \phi$  every turn. From  $w_0 = u_0\mathbf{Z}_0, \dots$ , we can see that  $\phi$  is determined by the initial value  $\mathbf{Z}_0$ .  $\mu$  represents the zero amplitude tune while  $\phi$  is the amplitude dependent tune-shift. Thus we get a set of new action-angle variables  $(r_j, \theta_j)$

$$w_j = |w_j|e^{i\theta_j} = r_j e^{i\theta_j}, j = 0, 1, \dots. \quad (11)$$

Even though all  $(r_j, \theta_j)$ 's behave like action-angle variables, they have different power orders of monomials of  $z, z^*$ , and hence represent approximation of the action-angle variable to different precisions. For example, in the case of a 7<sup>th</sup> order square matrix,  $w_0$  has terms of powers from 1<sup>st</sup> to 7<sup>th</sup> order,  $w_1$  has terms of powers from 3<sup>rd</sup> to 7<sup>th</sup> order while  $w_3$  has only a small 7<sup>th</sup> order term  $z(zz^*)^3$ .  $w_3$  provides little information about the rotation in the phase space while  $w_0$  has detailed information. In this paper, we only focus on  $w_0$ .

A stable motion means the invariant tori can survive with multiple turns. Applying Eq. (7)  $n$  times, we obtain

$$\mathbf{W}_n = e^{in\mu\mathbf{I}+n\tau}\mathbf{W}_0 = e^{in\mu}e^{n\tau}\mathbf{W}_0. \quad (12)$$

After a derivation based on Eq. (10) and (12), we recognize that a stable motion requires (see Eq.(1.19) of [1])

$$\text{Im}(\phi) \equiv \text{Im}\left(-\frac{iw_1}{w_0}\right) \approx 0; \Delta \equiv \frac{w_2}{w_0} - \left(\frac{w_1}{w_0}\right)^2 \approx 0. \quad (13)$$

We refer to Eq. (13) as the ‘‘coherence conditions’’ of a stable motion.  $w_0, \phi$ , and  $\Delta$  are all functions of the initial value of  $z, z^*$ . For a given initial value of  $|w_0|$ , the distortion of the real part of  $\phi$  from a constant is the tune fluctuation, while the imaginary part of  $\phi$  gives amplitude fluctuation, i.e., the variation of  $r_0 = |w_0|$  after many turns. The non-zero  $\Delta$  indicates a deviation from a coherent state, and it seems to be related to the Liapunov exponents [6] and the region of stable motion.

### III. APPLICATION

In this Section, we give an example of applying the square matrix method to optimize a storage ring’s dynamic aperture. Consider one particle with initial linear actions  $J_{x,y}$ . It is launched for multi-turns tracking. The linear actions are no longer constants when nonlinearity dominates over linear dynamics. There is a distortion from flat planes in the Poincaré section. We characterize this distortion by  $\Delta J/J = (J_{max} - J_{min})/J_{mean}$ . When the distortion is large, particles receive large nonlinear kicks and the motion becomes chaotic or even unstable. The stable region in phase space is defined as dynamic aperture. The goal of nonlinear optimization is to increase the dynamic aperture. In the 1D case, this is equivalent to optimizing the trajectories in the normalized phase space  $\bar{x} - \bar{p}_x$  so that they are as close as possible to circles (see FIG. 1, top right plot). In order to minimize  $\Delta J/J$ , we need to calculate  $J_{x,y}$  from constant  $|w_{x,y}|$ , in which an inverse function calculation is required. There is a way to avoid the inverse function calculation. Minimizing  $\Delta J/J$  is equivalent to optimizing the system so that constant planes in the Poincaré sections in  $J_{x,y}$  space are mapped to approximate flat planes in the Poincaré sections in the  $|w_{x,y}|$  space (see FIG. 2), and vice versa. Therefore we map a pair of constant  $J_{x,y}$  planes into a pair of surfaces of  $r_{x,y} = |w_{x,y}|$ . Then we characterize the nonlinear distortion by the deviation of surfaces of  $r_{x,y}$  from flat planes, given by

$$\frac{\Delta r}{\bar{r}} = \frac{\Delta|w|}{|\bar{w}|} = \frac{r_{max} - r_{min}}{\bar{r}}, \quad (14)$$

as a measure of nonlinearity. Here  $\bar{r}$  is the mean value of  $r$ . The system can be optimized by making the surfaces  $r_{x,y}$  as close as possible to constants for various amplitudes.

An application of this method was applied to the National Synchrotron Light Source-II (NSLS-II), when the lattice had a linear chromaticity of +7 in both planes. The lattice layout is described in ref. [27]. After tuning the chromaticity to +7 with 3 families of chromatic sextupoles, the optimization knobs were those 6 families of non-chromatic sextupoles. In this case we selected 3 sets of constant  $J_{x,y}$  in the  $J_{x,y} - \psi_x - \psi_y$  Poincaré section. In each set, we cast 64 initial coordinates uniformly distributed on the  $\psi_x - \psi_y$  plane. For every set of sextupole configuration, we calculated the new action  $r_{x,y}$  for all of the 3 sets of particles, using the formula  $w_0 = u_0 \mathbf{Z}_0$ . For each set, the nonlinearity measure from Eq. (14) was the optimization objective. In order to control the distortion for different sets simultaneously, we adopted the multi-objective genetic algorithm (MOGA) [28]. The choice of initial values was not unique. The question about how many sets should be used, and how many points should be cast inside each set is open for future exploration. After 85 generations and an evolution of 4000 populations, the optimizer converged to an optimal solution, which we labeled as Solution B in the following section.

Then we compared two solutions, A and B. Solution A is obtained by a conventional method - minimizing 8 first-order and 23 second-order nonlinear driving-terms, including amplitude-dependent-tune-shift [12, 29, 30]. Solution B was obtained using the square matrix method as outlined above. FIG. 2 shows that the square matrix method can significantly reduce the  $r = |w_0|$  distortions from a constant at a given initial amplitude  $x = 20mm$  and  $y = 3mm$ . As expected, we also observed that the trajectories of Solution B are much more linear than those of Solution A in the phase space (FIG. 1, top). The spectral analysis (FIG. 1, bottom) indicates that the motion in the case of Solution B is mainly dominated by a single frequency.

Here we note that the tune footprint (see FIG. 3) of Solution B has very large amplitude-dependent tune shift in both planes. It is remarkable that many particles can survive on a number of resonances at large amplitudes. FIG. 4 illustrates a simulated horizontal trajectory in phase space while its horizontal tune is almost exactly at a third order resonance. This indicates the irregularity near the resonance  $3\nu_x = n$ , has been almost completely eliminated. Usually  $3\nu_x$  is regarded as a dangerous resonance in a sextupole-dominated nonlinear lattice. For some machines, tunes can cross it at small amplitudes with no beam loss. When a particle's tune approaches the resonance, its amplitude will be blown-up and its tune is shifted off the resonance, which serves as a stability mechanism. The nonlinear force drives particles' tunes and amplitudes to vary, which leads to a visible tune diffusion and amplitude fluctuation [31]. In this case, the stop-band width is wide, and the motion stability is sensitive to errors. It is difficult for particles to cross the resonance at large amplitudes. In the past, the convention was to confine the tune footprint within a narrow range. The behavior of solution B, however, is

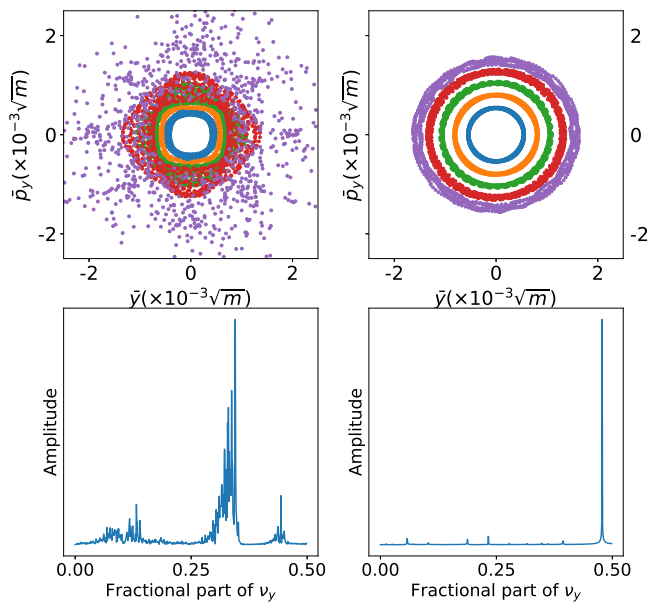


FIG. 1. Comparison of simulated trajectories (top) and spectral analysis (bottom) of  $\bar{y} - \bar{p}_y$  motion for Solution A (left) and Solution B (right). In both plots, 5 pairs of initial conditions with the  $x$  amplitude gradually increases from 10 to 20mm, and  $y$  increases proportional to  $x$  from 1 to 3mm. The spectral analysis for an initial condition  $x = 20mm$  and  $y = 3mm$  also indicates that Solution A's motion (bottom, left) is much more chaotic than B (bottom, right). The occupied area of Solution A becomes much larger for long-term tracking ( $> 15,000$  turns), but Solution B remains almost the same, which indicates the square matrix method is superior in optimizing the long term stability.

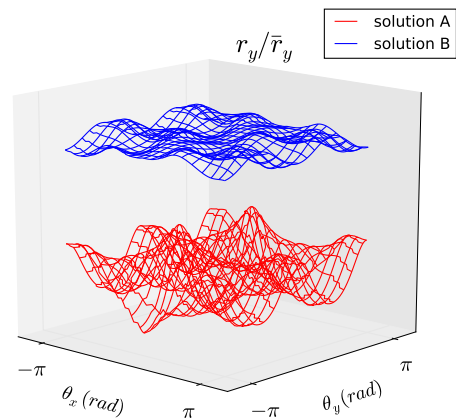


FIG. 2. Comparison of the distortion of  $r_y$  mapped from the same constant  $J_{x,y}$  planes for both solutions. Solution B plane is deliberately shifted up for a clear view.

very different than Solution A. FIG. 4 illustrates that

one particle can stably stay at the  $3\nu_x$  resonance without obvious tune diffusion and amplitude fluctuation at a large amplitude around  $x = 13.5\text{mm}$ . For each trajectory a unique tune is determined by its amplitude, but not the phase angle. Its nonlinear behavior is like a near-integrable system. Further exploration to understand nonlinear dynamic behavior in the vicinity of resonances is still under way.

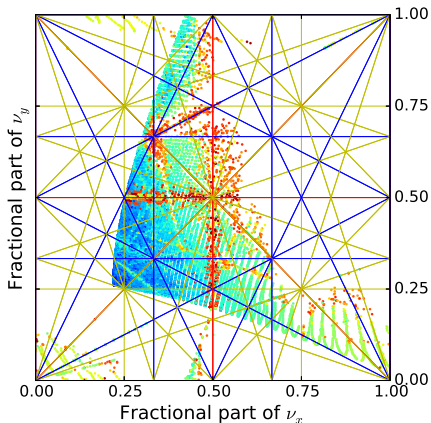


FIG. 3. Tune footprint for on-momentum dynamic aperture of Solution B. The color of each dot represents its tune diffusion  $\log_{10} \sqrt{\Delta\nu_x^2 + \Delta\nu_y^2}$  as defined in frequency map analysis [31, 32]. When the tune crosses the third order resonance  $3\nu_x = n$ , there is no beam loss, and even no obvious diffusion.

Our simulation shows that Solution B is quite tolerant to magnet imperfections. After the specified systematic and random multipole errors (the typical multipole components normalized to the main components evaluated at a  $25\text{mm}$  radius is around the order of  $1 - 3 \times 10^{-4}$  [33]), and some physical apertures limitation are introduced into the tracking simulation, the dynamic aperture remains sufficient for off-axis injection (see FIG. 5, right). In particular, particles can still cross the resonance  $3\nu_x = n$  smoothly, and the cancellation of resonance is well preserved (FIG. 4, bottom). Experimentally, under this sextupole configuration, 100% off-axis injection efficiency into the NSLS-II ring has been achieved, which is consistent with our analysis and simulation.

It is worth noting that when tight physical apertures are present in the storage ring, particles with a chaotic motion can be scraped by the boundary of the physical apertures, which results in a reduction of effective dynamic aperture. Regular motion is not limited in this way as can be seen in FIG. 5.

Over decades, we have followed a common convention – choosing the fractional tunes far away from low-order resonances. With this design, sextupoles are tuned to confine amplitude-dependent tune-shift in order to avoid crossing them. The solution obtained with our method, however, obviously violates this convention. This indicates that confining tune footprint in order to avoid res-

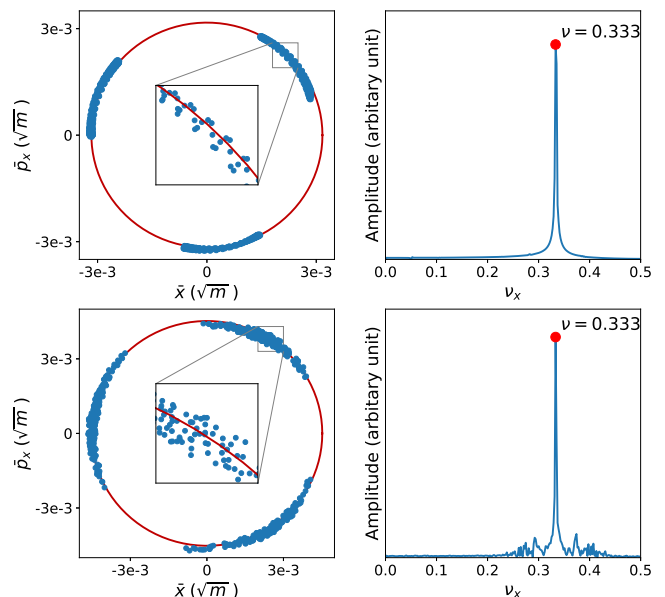


FIG. 4. Simulated horizontal phase space trajectories with their tunes at a third order resonance. In the left plots and their zoomed-in subplots, the red lines represent constant linear actions. The blue dots are the simulated turn-by-turn data. The frequency spectrums (right) indicates that the particle can stably stay at the resonance line. The top plots are for an ideal machine, and the bottom plots for the machine with errors.

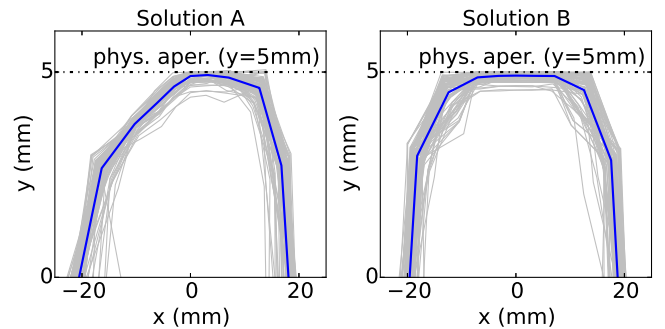


FIG. 5. Comparison of effective dynamic apertures of two Solutions when a physical aperture limitation  $y = 5\text{mm}$  and multipole errors are present. The blue lines are the aperture averaged over 80 random seeds (light-gray lines). The top-left corner of Solution A's aperture is scraped due to the chaotic vertical motion.

onance line-crossing is not absolutely necessary in lattice optimization. Our method suggests a new lattice design philosophy, where instead of confining tune footprint excursion, one can tune sextupoles to minimize the variation of  $r_{x,y} = |w_{x,y}|$  at different amplitudes to optimize dynamic aperture.

#### IV. CONCLUSION

Through the use of linear algebra techniques we developed a new method for analyzing periodic, nonlinear dynamical systems. Applying Jordan decomposition to the eigenspace of the square matrix, we found a set of accurate action-angle variables. The distortions from the flat planes after mapping constant linear actions to the new actions are one measure of nonlinearity. Several other measures, such as the two measures given by Eq. (13) could be used in future exploration. Our method was successfully field-tested by optimizing the NSLS-II lattice. Most importantly, optimization using our square matrix method has generated an unprecedented nonlinear lattice which allows particles to stay exactly on resonance. Thus the new approach allows relaxed tune footprint, and widely opened a potential new direction for

the search of larger dynamic aperture. It also provides a different perspective to guide the understanding of the nonlinear dynamics. The square matrix method is general and can be applied to other nonlinear dynamical systems with periodic structure, such as celestial mechanics.

#### ACKNOWLEDGMENTS

We would like to thank Dr. Y. Hao for sharing his TPSA code, Dr. B. Nash for the collaboration during the early stage of developing this method, Dr. M. Borland and Dr. Y.P. Sun for discussion and collaboration on applying this method to the APS-U ring, Dr. X. Huang for implementing experimental studies on the SPEAR3 ring, Prof. A. Chao for a stimulating discussion, and Mr. R. Rainer for editing the manuscript. This work was supported by Department of Energy Contract No. DE-AC02-98CH10886 and DE-SC0012704.

- 
- [1] L. H. Yu, Phys. Rev. Accel. Beams **20**, 034001 (2017).
  - [2] L. H. Yu and B. Nash, in *PAC'09* (2010) p. TH6PFP067.
  - [3] H. Yoshida, Phys. Lett. **A150**, 262 (1990).
  - [4] M. Borland, ANL/APS/LS-287 (2000).
  - [5] F. Schmidt, PAC'05 Conf. Proc. (2005).
  - [6] A. J. Lichtenberg and M. A. Leiberman, *Regular and chaotic dynamics*, Applied mathematical sciences (Springer, 1992).
  - [7] R. D. Ruth, AIP Conf. Proc. **153**, 150 (1987).
  - [8] G. Guignard, CERN-78-11 (1978).
  - [9] A. Schoch, CERN-57-21 (1958).
  - [10] A. J. Dragt, AIP Conf. Proc. **177**, 261 (1988).
  - [11] M. Berz, IEEE PAC Conf. Proc. 89 , 1419 (1989).
  - [12] A. Chao, SLAC-PUB-9574 (2002).
  - [13] A. Bazzani, E. Todesco, G. Turchetti, and G. Servizi, CERN-94-02 (1994).
  - [14] E. Forest, M. Berz, and J. Irwin, Part. Accel. **24**, 91 (1989).
  - [15] L. P. Michelotti, *Intermediate classical dynamics with applications to beam physics* (Wiley, 1995).
  - [16] E. Forest, *Beam Dynamics: A New Attitude and Framework*, Vol. 8 (Hardwood Academic / CRC Press, 1998).
  - [17] Y. Cai, Nucl. Instrum. Meth. **A645**, 168 (2011).
  - [18] W. Wan and J. R. Cary, Phys. Rev. ST Accel. Beams **4**, 084001 (2001).
  - [19] V. Danilov and S. Nagaitsev, Phys. Rev. ST Accel. Beams **13**, 084002 (2010).
  - [20] B. Autin, AIP Conf. Proc. **153**, 288 (1987).
  - [21] J. Hagel, CERN-LEP-TH/87-15 (1987).
  - [22] E. D. Courant and H. S. Snyder, Annals Phys. **3**, 1 (1958), [Annals Phys.281,360(2000)].
  - [23] S. Y. Lee, *Accelerator physics* (1999).
  - [24] J. Pöschel, Pure Math. **69** (2001).
  - [25] R. J. Glauber, Phys. Rev. **131**, 2766 (1963).
  - [26] E. C. G. Sudarshan, Phys. Rev. Lett. **10**, 277 (1963).
  - [27] BNL, <https://www.bnl.gov/nsls2/project/PDR/>.
  - [28] K. Deb, A. Pratap, S. Agarwal, and T. Meyerivan, Trans. Evol. Comp **6** (2002).
  - [29] Y. Li and L. Yang, Int. J. Mod. Phys. **A31**, 1644019 (2016).
  - [30] C. X. Wang, ANL/APS/LS-330 (2012).
  - [31] J. Laskar, PAC'03 Conf. Proc. (2003).
  - [32] D. Robin, C. Steier, J. Laskar, and L. Nadolski, Phys. Rev. Lett. **85**, 558 (2000).
  - [33] J. Skaritka et al., in *PAC'09, Vancouver, Canada, May, 2009* (2010).